Crystal structure of peptidyl-tRNA hydrolase from a Gram-positive bacterium, *Streptococcus pyogenes* at 2.19 Å resolution shows the closed structure of the substrate-binding cleft

Avinash Singh, Lovely Gautam, Mau Sinha, Asha Bhushan, Punit Kaur, Sujata Sharma, T.P. Singh *

Department of Biophysics, All India Institute of Medical Sciences, New Delhi, India

ABSTRACT

Peptidyl-tRNA hydrolase (Pth) catalyses the release of tRNA and peptide components from peptidyl-tRNA molecules. Pth from a Gram-positive bacterium *Streptococcus pyogenes* (*Sp*Pth) was cloned, expressed, purified and crystallised. Three-dimensional structure of *Sp*Pth was determined by X-ray crystallography at 2.19 Å resolution. Structure determination showed that the asymmetric unit of the unit cell contained two crystallographically independent molecules, designated A and B. The superimposition of C^α traces of molecules A and B showed an r.m.s. shift of 0.4 Å, indicating that the structures of two crystallographically independent molecules were identical. The polypeptide chain of *Sp*Pth adopted an overall α/β conformation. The substrate-binding cleft in *Sp*Pth is formed with three loops: the gate loop, Ile91–Leu102; the base loop, Gly108–Gly115; and the lid loop, Gly136–Gly150. Unlike in the structures of Pth from Gram-negative bacteria, the entry to the cleft in the structure of *Sp*Pth appeared to be virtually closed. However, the conformations of the active site residues were found to be similar.

1. Introduction

The translation of genetic information by mRNA to ribosome often gets terminated due to a variety of reasons [1–4]. The premature termination results in the release of peptidyl-tRNA molecules which are toxic to the cell [5–8]. The loss of tRNA molecules to such a by-product reduces the availability of free tRNAs. This affects the protein synthesis adversely. However, such a condition can be corrected by an enzyme known as peptidyl-tRNA hydrolase (Pth). It has been shown by mutation studies that this enzyme is essential for the survival of bacteria [9]. Pth is an esterase which catalyses the release of peptide and tRNA components from peptidyl-tRNA molecule by cleaving it at the ester bond. Pth was first identified in *Escherichia coli* [10,11]. Later on, it was reported in yeast [12] and subsequently in other bacteria as well including *Streptococcus pyogenes* [13]. Actually, there are several types of

Pth enzymes [14], Pth1 is found in the cells of bacteria and eukaryotes [15–17] while Pth2 is found in archaea and eukaryotes [18–20]. In eukaryotes, both Pth1 and Pth2 as well as some additional types of Pth enzymes are present [14,18,19]. While Pth1 is essential in bacteria for restoring the translational function of ribosome [9,17], it is not absolutely essential in eukaryotes [17–19]. Pth1 consists of approximately 190 amino acid residues while archaeal Pth2 has approximately 120 amino acid residues [21,22] and human Pth2 enzyme has 116 amino acid residues [23]. Structurally also, Pth1 is significantly different from archaeal Pth2 [21,22] and human Pth2 enzymes [23]. Since the present paper deals with the investigations on bacterial Pth1 enzyme only, it will be referred hereafter as Pth.

So far, crystal structures of Pth enzymes are available from a few Gram-negative bacteria including *E. coli* (*Ec*Pth) (PDB: 2PTH, 3VJR) [24], *Acinetobacter baumannii* (*Ab*Pth) (PDB: 3WH4, 4JWK, 4JX9) [25], *Pseudomonas aeruginosa* (*Pa*Pth) (PDB: 4JC4, 4FYJ) [26,27], *Francisella tularensis* (*Ft*Pth) (PDB: 3NEA) [28] and *Burkholderia thailandensis* (*Bt*Pth) (PDB: 3V2I) [29]. In addition to these structures, crystal structures of Pth enzymes from *Mycobacterium tuberculosis* (*Mt*Pth) (PDB: 2Z2I) [30] and *Mycobacterium smegmatis* (*Ms*Pth) (PDB: 3KJZ) [31] are also known. However, so far, no structure of Pth from any Gram-positive bacteria is known. We report here, the first crystal structure of Pth from a Gram-positive

bacterium, *S. pyogenes* (*Sp*Pth). *Sp*Pth shows sequence identities ranging from 30% to 32% (Fig. 1) with Pth enzymes of other bacteria whose structures are known [24–31]. The three-dimensional structure of *Sp*Pth has been determined at 2.19 Å resolution.

2. Results

2.1. Overall structure

The structure determination of *Sp*Pth revealed the presence of two crystallographically independent molecules, A and B in the asymmetric unit. Each molecule consists of 189 amino acid residues. Molecules A and B were arranged side-by-side with a buried surface area of 535 Å². They formed three intermolecular hydrogen bonds and several van der Waals contacts. However, the gel-filtration profile of *Sp*Pth (Fig. S1A), when compared with a calibration

curve obtained using proteins of known molecular weights (Fig. S1B), indicated a molecular weight of about 24 kDa. It suggested that *Sp*Pth did not form a stable dimer in solution. Thus, the association of two crystallographically independent molecules in the crystals may not be considered as a dimer.

The r.m.s. shift of 0.4 Å was obtained when C^{α} traces of the two crystallographically independent molecules, A and B were superimposed on each other. It showed that the structures of molecules, A and B were identical. Therefore, hereafter only one molecule will be used in the subsequent discussion. The structure of *Sp*Pth consisted of six α-helices and seven β-stands (Fig. 2A). Four parallel β-strands, β4, β1, β5 and β7 formed a twisted β-sheet in the centre of the molecule. The antiparallel β-strands, β2 and β3 cross the sheet at the centre. The β-strand β6 is antiparallel to β-strand, β7 and parallel to the longest α-helix, α5 in the structure. The β-structure is surrounded from three sides by α-helices among
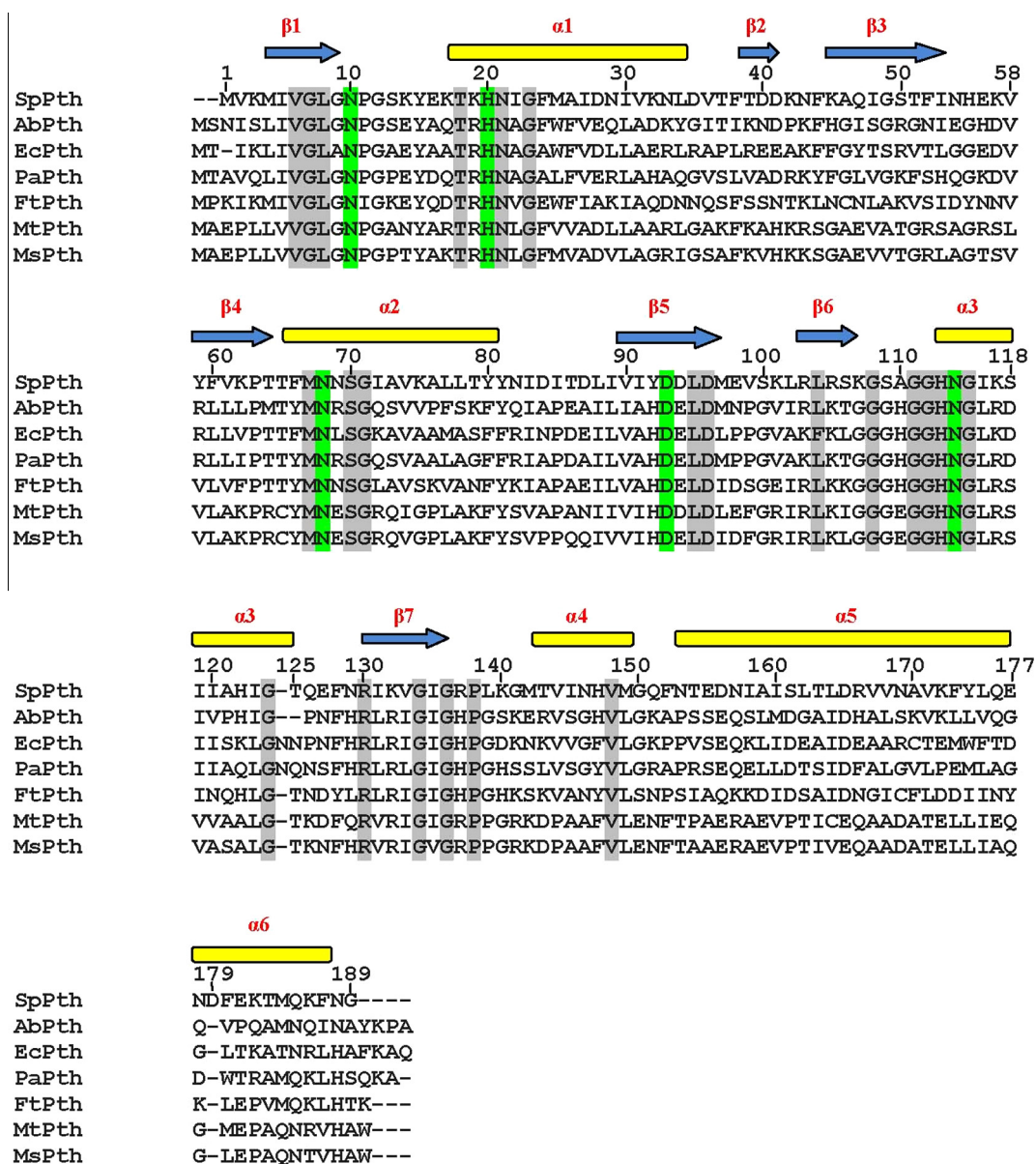
Fig. 1. Sequence alignment of *Sp*Pth enzyme with Pth enzymes from other bacteria including *Ab*Pth (32%), *Ec*Pth (31%), *Pa*Pth (31%), *Ft*Pth (31%), *Mt*Pth (30%) and *Ms*Pth (30%) where sequence identities are given in parentheses. The fully conserved residues are highlighted in grey. The suggested active site residues are highlighted in green. The positions of secondary structure elements are shown as arrows (β-strands) and cylinders (α-helices). (For interpretation of the references to colour in this figure legend, the reader is referred to the web version of this article.)

Fig. 2. (A) Overall structure of SpPth in ribbon representation. Secondary structure elements, α-helices, 1–6 and β-strands, 1–7 are labelled. (B) Superimpositions of Cᵅ traces of SpPth (green) and AbPth (grey) showing variations in the paths of their polypeptide chains. The r.m.s. shift in the positi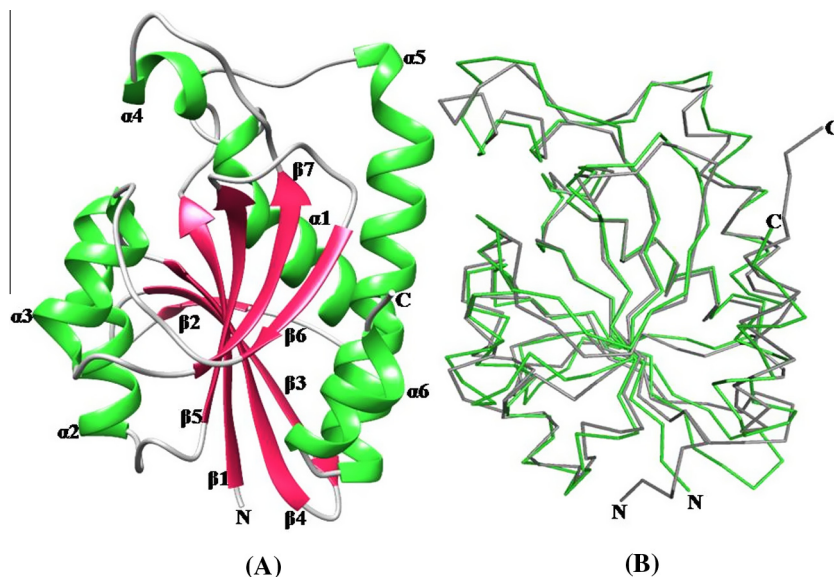ons of Cᵅ atoms of the two structures was found to be 1.6 Å. (For interpretation of the references to colour in this figure legend, the reader is referred to the web version of this article.)

which two α-helices, α2 and α3 provided a cover from one side while α5 and α6 are located on the opposite side of α2 and α3. The α-helix, α1 covers the β-sheet structure from the third side. The fourth side is open and may be required to allow the hinge motion involving the β-sheet. The residues of N-terminus are predominantly hydrophobic in nature while those at the C-terminus are hydrophilic. It may be mentioned here that the structures of N- and C-terminal segments were clearly defined in the electron densities.

The structure of AbPth (PDB: 3WH4) was used for comparison as it represented a native unbound state of Pth from Gram-negative bacteria and also has the maximum sequence identity of 32% with SpPth. The superimposition of Cᵅ traces of SpPth on those of AbPth gave an r.m.s. shift of 1.6 Å indicating an appreciable deviation between the paths of polypeptide chains of two Pth enzymes representing two different classes of bacteria (Fig. 2B). In contrast, the corresponding r.m.s. shifts among Cᵅ traces of Pth enzymes belonging to Gram-negative bacteria [24–29] were found to be in the range of 0.7–1.4 Å. It showed that the path of the polypeptide chain of a Pth enzyme from a Gram-positive bacterium differed slightly from those of Gram-negative bacteria.

The values of length and width of the molecular structure of SpPth as estimated in terms of distance between His55 Cᵅ on one end and Gly141 Cᵅ on the opposite end and the distance between Lys42 Cᵅ belonging to one side and Gln185 Cᵅ belonging to the opposite side were 49.6 Å and 36.2 Å, respectively. The corresponding values in the structure of AbPth were found to be 44.7 Å and 35.8 Å, respectively. However, it may be mentioned here that both regions to which His55 and Lys142 belonged have higher values of B factors as compared to the rest of the protein. This may be due to conformational flexibility.

2.2. Substrate binding cleft

The substrate binding cleft in Pth enzymes is formed with three segments, a base loop, Gly108–Gly115, a gate loop, Ile91–Leu102 and a lid loop, Gly136–Gly150 (Fig. 3A1). The base loop forms one side of the cleft while lid loop and gate loop form the opposite side of the cleft. The minimum distance from any atom of the base loop, Gly108–Gly115 to any atom of lid loop, Gly136–Gly150 in the

native unbound state of SpPth was found to be 3.47 Å. This showed that the structure of SpPth in the native unbound state had the narrowest opening between the base and the lid loops among all the known structures of Pth enzyme reported so far (Table 2A). Similarly, the shortest distance between any atom of base loop, Gly108–Gly115 and any atom of gate loop, Ile91–Leu102 was found to be 3.88 Å. The width of the gate in SpPth was found to be smaller than those observed in Pth enzymes of Gram-negative bacteria (Table 2B). Only in the case of MtPth, the corresponding distance of 3.33 Å was smaller than that of SpPth (Table 2B).

Furthermore, in the structure of SpPth, the residues from opposite sides of the cleft formed several van der Waals contacts (Fig. 3A2). These distances indicated that the substrate binding cleft was closed at both lid and gate loops as well as the region between the closed lid loop and the closed gate loop (Fig. 3B1). In MtPth, it is fully closed at the gate loop but it is wide open at the lid loop (Fig. 3B2). On the other hand, the substrate binding channel in EcPth is wide open as both lid and gate loops are away from the base loop (Fig. 3B3). It shows that the catalytic site in the structure of SpPth appeared to be inaccessible. For the catalytic action to occur, the lid loop, Gly136–Gly150 and the gate loop Ile91–Leu102 will have to move away from their respective positions in the native state for the substrate to reach the active site residues. As seen from the superimposition of substrate binding clefts of SpPth (green) and EcPth (grey) (Fig. 4) together with the bound C-terminal tripeptide from the neighbouring molecule in EcPth, there were steric constraints for the binding of such a peptide in the native state of SpPth. This further indicated that the binding of ligands in the substrate binding cleft in SpPth may occur only if the lid loop, Gly136–Gly150 and the gate loop, Ile91–Leu102 moved away considerably.

2.3. Catalytic site

The structural and point mutation studies have suggested that the amino acid residues, His20, Asp93, Asn10, Asn68 and Asn114 may play a role in the catalytic action of Pth enzymes [24,32–34]. The structural studies of the complexes of AbPth and PaPth with ligands have also shown that residues, Asn10, His20, Ans68 and Asn114 are involved in the binding with ligands in the
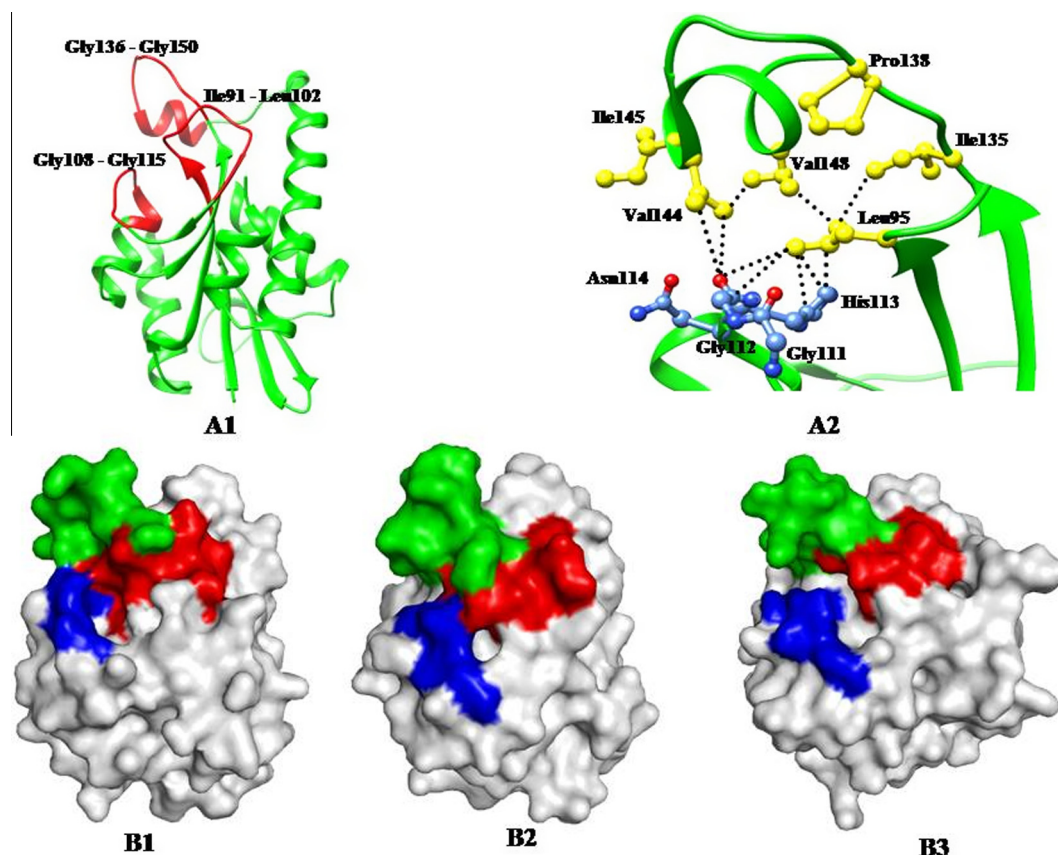
Fig. 3. (A1) The segments Gly108–Gly115, Ile91–Leu102 and Gly136–Gly150 of the substrate binding cleft (red). The segment Gly108–Gly115 represents the base loop while segments Gly136–Gly150 and Ile91–Leu102 represent lid and gate loops, respectively. (A2) The residues protruding into the substrate binding cleft in *Sp*Pth. The residues in blue belong to the base loop of the cleft while those in yellow belong to the lid and gate loops. Dotted lines indicate van der Waals contacts. (B) Molecular surfaces of Pth enzymes with base loop (blue), lid loop (green) and gate loop (red) showing that the substrate binding cleft in (B1) *Sp*Pth, closed at both lid and gate loops, (B2) *Mt*Pth, closed at gate loop but wide open at lid loop and (B3) *Ec*Pth, fully open channel both at both lid and gate loops. (For interpretation of the references to colour in this figure legend, the reader is referred to the web version of this article.)

substrate binding cleft [25,27]. However, Out of these residues, the conformation of the side chain of Asn114 was found to be very sensitive when Pth interacted with other molecules through the substrate binding cleft. The torsion angle, χ^1 of 63° for the side chain of Asn114 as observed in the structure of *Sp*Pth defined the conformation of Pth in the native unbound state. The value of the corresponding torsion angle in the native unbound state of *Ab*Pth [PDB: 3WH4] was 69°. Also, in the structure of the complex of *Ec*Pth with tRNA CCA-acceptor-TΨC domain [34] in which there are no interactions with the active site region, the value of corresponding torsion angle, χ^1 was 60°. Similarly, the values of 63° and 97° were observed for the corresponding torsion angles in the native structures of *Mt*Pth [30] and *Ms*Pth [31], respectively. These values clearly indicated that the torsion angle, χ^1 for the side chain of Asn114 in the native unbound state of Pth was centred at 60°. Upon ligand binding to Pth at the substrate binding cleft, the conformation of the side chain of Asn114 changed in which the new values of the torsion angle, χ^1 were centred at −60° [24,25,27]. Based on these observations, it may be concluded that the conformation of the side chain of Asn114 in the unbound state adopted a conformation with values of torsion angle, χ^1 centred at 60°. This conformation favoured the formation of a hydrogen bond between Asn114 and His20. On the other hand, in the ligand bound state, the side chain of Asn114 adopted a conformation with values of torsion angle, χ^1 centred at −60°. In this state, the side chain of Asn114 turned away from His20 and the hydrogen bond between Asn114 and His20 was lost. In other words, the conformation of the

side chain of Asn114 provided a clear indication about the binding state at the substrate binding site in Pth.

3. Discussion

The structure determination of *Sp*Pth revealed that the gate loop, Ile91–Leu102 and the lid loop, Gly136–Gly150 formed one side of the cleft while the base loop, Gly108–Gly115 represented the opposite wall. It may be mentioned here that all the three loops in the structure of *Sp*Pth had well defined structures with values of 16 Å² for the average B factors. The lid loop, Gly136–Gly150 in *Sp*Pth is internally well stabilized with a number of intra-loop interactions (Fig. 5A). The segment, Val144–Met149 of this loop was found to adopt a stable α-helical structure which was stabilized by hydrogen bonds, Val144 O···N Val148 = 2.95 Å and Ile145 O···N Met149 = 2.85 Å. A tetra peptide of this loop, Leu139–Lys140–Gly141–Met142 formed a tight type II β-turn structure with a hydrogen bond between Leu139 O···N Met142 = 3.04 Å. In the same loop, another hydrogen bond was formed between Gly136 O and His147 N$^{\varepsilon 2}$ at a distance of 2.95 Å. Additionally, the side chain of Pro138 was stacked with the aromatic ring of His147. Similarly, the gate loop, Ile91–Leu102 (Fig. 5B) was also well stabilized in the structure of *Sp*Pth. In this loop, a tetra peptide, Asp94–Leu95–Asp96–Met97 adopted a type I β-turn conformation which was stabilized by a hydrogen bond formed between Asp94 O$^{\delta 2}$ and Met97 N. An intra-residue hydrogen bond was also observed between Asp96 O$^{\delta 2}$ and Asp96
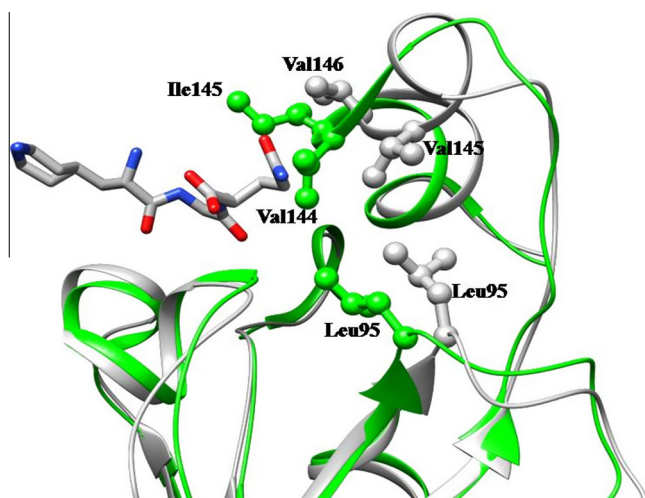
Fig. 4. Superimpositions of substrate binding clefts of *Sp*Pth and *Ec*Pth. *Sp*Pth is shown in green while *Ec*Pth is shown in grey. The C-terminal tripeptide (grey) from the neighbouring molecule from the structure of *Ec*Pth (PDB ID: 2PTH) [24] is overlayed on it. It shows that the bound tripeptide of neighbouring molecule in the structure of *Ec*Pth is not compatible with the stereochemistry of the substrate binding cleft in the structure of *Sp*Pth due to steric constraints from the residues of the lid loop. (For interpretation of the references to colour in this figure legend, the reader is referred to the web version of this article.)

N. Similar tight β-turn was not observed in the structures of other Pth enzymes [24–31] due to specific amino acid sequence differences in the corresponding loops. Furthermore, due to these tight β-turns in the loops, Ile91–Leu102 and Gly136–Gly150, the paths of the polypeptide chain after the β-turns in *Sp*Pth differed significantly from that reported in the native unbound structure of *Ab*Pth (Fig. 6A). Also such a conformation was found to influence the positions of the side chains of Leu95 and Val144 which shifted towards the base loop, Gly108–Gly115. It reduced the free space in the substrate binding cleft. The comparison of distances between Val144 of lid loop and Gly112 of base loop in various Pth enzymes are given in Table 2A. These distances indicated that the positions of the lid loops in various Pth enzymes varied considerably. The observed van der Waals contacts involving residues, Val144 and Leu95 with the atoms of the base loop, Gly108–Gly115 from the

opposite side of the cleft (Fig. 3A2) and showed that the substrate binding cleft in *Sp*Pth was packed somewhat differently.

The substrate binding cleft in *Sp*Pth is expected to open on ligand binding where both the gate loop, Ile95–Leu102 and the lid loop, Gly136–Gly150 will be required to move away from their closed positions so that the substrate could align with the catalytic residues. Due to tight internal packings of these two loops in the structure of *Sp*Pth, the lid loop may have slightly different movement from those observed in other Pth enzymes where the corresponding loops are relatively more flexible [24–31].

Previously, in the structures of Pth enzymes of various bacteria, the distances between Gly113 C^{α} and Asp98 $O^{\delta 2}$ were described to determine the widths of the gate [25,26,30,31]. In the present structure, the side chain of corresponding residue Asp96 occupied a different position because Asp96 $O^{\delta 1}$ formed a hydrogen bond with Arg137 N^{ϵ} (Fig. 6B). As a result of this, the distance estimated for the width of the cleft with respect to Asp96 $O^{\delta 2}$ in *Sp*Pth was not the shortest distance. In this case, the shortest distance was provided by Leu95 $C^{\delta 1}$. The corresponding interaction involving Asp96 is not present in Pth enzymes of Gram-negative bacteria because those enzyme consisted of His138 instead of Arg137 [24–29]. Although in *Mt*Pth and *Ms*Pth, the corresponding residue is Arg139, it still occupied a different position in the structure because it followed a slightly different chain path due to a unique sequence of Pro139–Pro140 [30,31]. The corresponding sequence in *Sp*Pth is Pro138–Leu139 while in Pth of Gram negative bacteria, it is Pro139–Gly140 [24–29]. Due to such variations in the nature of interactions involving Asp96, the side chain of Asp96 may occupy different positions. Thus, using Asp96, as used previously in the structures of Pth enzymes [25,26,30,31] as a reference residue for the determination of the width of the gate to the substrate binding site did not provide an accurate generalisation. The actual estimation of the width of the gate should be based on the criterion of the shortest distance between any atom of the base loop, Gly108–Gly115 and any atom of the gate loop, Ile91–Leu102. The comparison of these distances in Pth structures are given in Table 2B. It is interesting to note that the shortest distance in *Sp*Pth is between Gly112 and Leu95 while in rest of the structures, the shortest distances are estimated between Gly111/Gly113 and Asp96/Asp98.

It may also be mentioned here that the structure of *Sp*Pth is the first structure of Pth enzyme from a Gram-positive bacterium. It
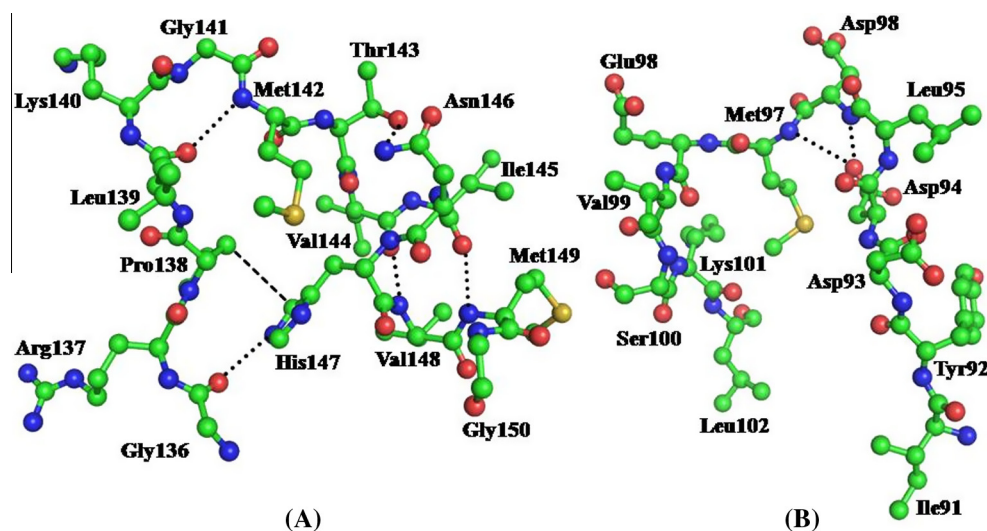
Fig. 5. (A) The lid loop, Gly136–Gly150 containing an α-helical segment (Val144–Met149) and a tight β-turn segment (Leu139–Met142) with several intra-loop hydrogen bonds which are indicated by dotted lines. A notable van der Waals contact distance of 3.77 Å between Pro138 C^{β} and His147 $C^{\delta 2}$ is indicated by a dashed line. (B) The gate loop, Ile91–Leu102 contains a tight β-turn segment (Asp94–Met97). The loop is stabilized by two hydrogen bonds and several van der Waals contacts.

Fig. 6. (A) The superimpositions of the regions consisting of loops, Gly108–Gly115, Ile91–Leu102 and Gly136–Gly150 of *Sp*Pth (green) on *Ab*Pth (grey). The comparison shows that the residues in *Sp*Pth occupy significantly d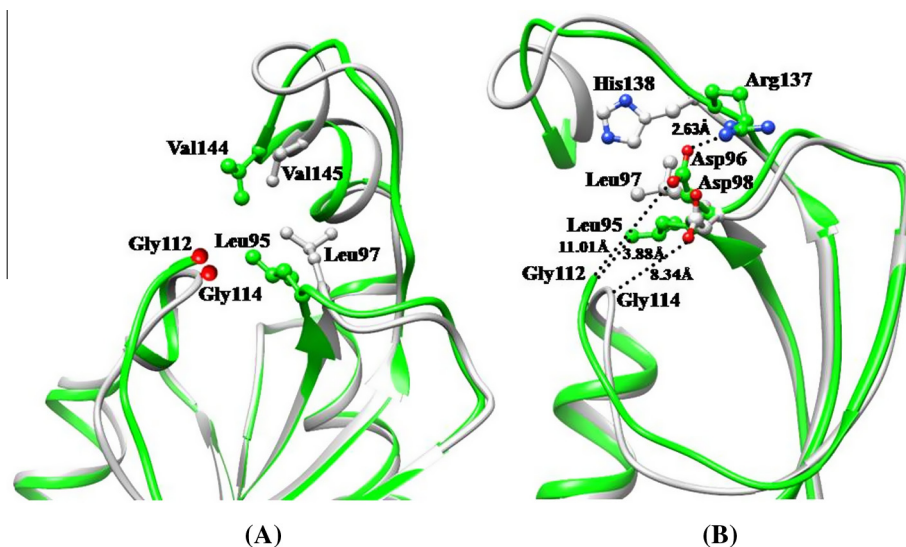ifferent positions in the cleft and form van der Waals contacts involving inter-loop residues. (B) The interactions of Asp96 in *Sp*Pth (green) and of the corresponding Asp98 in *Ab*Pth (grey) are shown. Asp96 in *Sp*Pth forms an ionic interaction with Arg137 while Asp98 of *Ab*Pth is not involved in such an interaction. As a result, Asp96 in *Sp*Pth, has moved away from Gly112 of the base loop Gly108–Gly115. The residue corresponding to Arg137 of *Sp*Pth is His138 in *Ab*Pth and other enzymes from Gram-negative bacteria. (For interpretation of the references to colour in this figure legend, the reader is referred to the web version of this article.)

revealed notable differences in the structural features of the lid and gate loops when compared with those of other Pth enzymes. The region between the lid and gate loops was found to be tightly packed. Also the structure of *Sp*Pth provided a new rationalisation for the measurements of the width of the gate. The structure determination also revealed that the substrate binding cleft is obstructed at two positions, one by the lid loop and by the gate loop. The overall variations in the structures of the substrate binding clefts of Pth enzymes from various bacteria may be helpful in the designing of specific inhibitors against the enzymes of different bacteria.

4. Materials and methods

4.1. Cloning, expression and purification of SpPth

The freeze dried culture of *S. pyogenes* was obtained from CSIR-Institute of Microbial Technology, Chandigarh (India) with Microbial Type Culture Collection (MTCC) Number 1924. From this, the genomic DNA was isolated and the Pth gene was amplified using the forward Fw 5′-CGGGATCCATGGTAAAAATGATTGTTGGTC-3′ and reverse Rw 5′-CCGCTCGAGTTATCCATTAAATTTCTGCATTG-3′ primers. The forward and reverse primers contained *BamH1* and *Xho1* restriction sites, respectively. The amplified gene was cloned into pGEMT-easy cloning vector and sub-cloned into pET-28a⁺ expression vector. The sequence of the constructed plasmid was verified by DNA sequencing. The verified plasmid was introduced into *E. coli* BL21 (DE3) expression system.

A single freshly transformed colony was inoculated in 10 ml LB (Luria–Bertani) containing 100 µg/ml kanamycin and was kept in water bath overnight at 37 °C in shaking condition. 1% culture from primary inoculation was added in 1000 ml LB medium containing 100 µg/ml kanamycin and kept in orbital shaker at 37 °C in shaking condition until the optical density (OD) of the culture at 600 nm reached the level of 0.4–0.6. 5 ml of this secondary culture were removed and kept at 4 °C as an uninduced culture. The remaining secondary culture of recombinant cells containing the insert was induced with 0.4 mM isopropyl-1-thio-β-D-galactopyranoside (IPTG) at 20 °C for 16 h. The cells were harvested by centrifugation at 9803*g* for 15 min.

The cell pellet was dissolved in 50 mM Tris–HCl buffer containing 300 mM NaCl and 10 mM imidazole, pH 8.0, 1 mM protease inhibitor cocktail (Roche, Basel, Switzerland). The cells were disrupted using sonicator (Model UP50H, Hielscher, Brandenburg, Germany). The cleared lysate was applied to an Ni-NTA Super-flow column (Qiagen, Hilden, Germany) which was pre-equilibrated in lysis buffer containing 50 mM Tris–HCl buffer, 300 mM NaCl and 10 mM imidazole, pH 8.0 and purified using stepwise washing with 30 mM imidazole followed by 300 mM imidazole in lysis buffer. The eluted fractions were examined using 10% sodium dodecyl sulphate–polyacrylamide gel electrophoresis (SDS–PAGE). A single band of protein corresponding to molecular weight of approximately 24 kDa was observed. The final purification step was carried out using gel filtration chromatography with Sephadex G-50 column. The purity of the protein was established using SDS–PAGE which showed a single band at approximate molecular weight of 24 kDa.

4.2. Crystallisation of SpPth

The freshly prepared sample of purified protein was used for crystallization with hanging drop vapour-diffusion method at 298 K using 24 well linbro crystallization plates. The initial crystallization screening experiments were carried out using Hampton Research crystallization kit (HR2110–HR2112). The protein concentration was set to 16 mg/ml in 50 mM HEPES buffer, pH 6.5. The crystals of *Sp*Pth were obtained by equilibrating 4 µl protein drops (containing 2 µl protein solution and 2 µl reservoir solution) against a reservoir solution containing 25% (v/v) PEG 10,000 and 50 mM HEPES buffer, pH 6.5. The crystals grew to approximate dimensions of $0.4 \times 0.4 \times 0.4$ mm³ in about 2 weeks.

4.3. X-ray intensity, data collection and processing

Crystals of *Sp*Pth were stabilized by adding 25% glycerol to the mother liquor for data collection at low temperature. A single crystal was mounted in a nylon loop and flash-frozen in liquid nitrogen. The data were collected at 100 K on MAR 225 CCD detector (MAR RESEARCH, Norderstedt, Germany) using beamline, BM14 at ESRF, Grenoble, France. A complete data set was collected using

Table 1
Crystallographic data for Peptidyl-tRNA hydrolase from *Streptococcus pyogenes* at 2.19 Å resolution. Values in parentheses are for the highest resolution shell.

Data collection statistics	
Space group	P1
Unit-cell dimensions	
a (Å)	36
b (Å)	43
c (Å)	65.1
α (°)	90.3
β (°)	105.7
γ (°)	112.5
Number of molecules in unit cell	2
V_m (Å^3/Da)	2
Solvent Content (%)	41.3
Resolution range (Å)	35.40–2.19
No. of measured reflections	64,832
No. of unique reflections	17,325
Overall completeness (%)	98.3 (97.3)
R_{sym} (%)	6.2 (15.7)
$I/\sigma(I)$	22.2 (7.6)
Redundancy	3.7 (3.2)
Refinement statistics	
R_{cryst} (%)	16.8 (19.7)
R_{free} (5% data) (%)	19.8 (21.6)
Number of protein atoms	2980
Number of water oxygen atoms	281
r.m.s. deviations	
Bond length (Å^2)	0.014
Bond angles (°)	1.6
Dihedral angles (°)	17.6
Mean B factor (Å)^2 for	
Main chain atoms	15.5
Side chain and water oxygen atoms	19.8
Overall	17.8
Ramachandran plot statistics	
Residues in the most favoured regions (%)	93.2
Residues in the additionally allowed regions (%)	6.2
Residues in the disallowed regions (%)	0.6 (Phe68 A, Phe68 B)

Table 2A
A comparison of the minimum distances between the atoms of the base loop, Gly108–Gly115 and the lid loop, Gly136–Gly150 in the structures of various bacterial Pth enzymes.

Protein	Residues	Distances (Å)
*Sp*Pth	Gly112 O$\cdots$Val144 C$^{\gamma 1}$	3.47
*Pa*Pth	Gly114 O$\cdots$Val145 C$^{\gamma 2}$	6.68
*Ab*Pth	Gly114 O$\cdots$Val145 C$^{\gamma 2}$	7.44
*Ec*Pth	Gly114 O$\cdots$Val145 C$^{\gamma 2}$	7.03
*Mt*Pth	Gly114 O$\cdots$Pro146 C$^{\beta}$	6.95
*Ms*Pth	Gly114 O$\cdots$Pro146 C$^{\beta}$	6.29
*Ft*Pth	Gly114 O$\cdots$Val146 C$^{\gamma 1}$	6.98

Table 2B
A comparison of minimum distances between the atoms of the base loop, Gly108–Gly115 and the gate loop, Ile91–Leu102 in the structures of various bacterial Pth enzymes.

Protein	Residues	Distances (Å)
*Sp*Pth	Gly112 O$\cdots$Leu95 C$^{\delta 1}$	3.88
*Ab*Pth	Gly113 O$\cdots$Asp98 O$^{\delta 2}$	4.89
*Pa*Pth	Gly113 O$\cdots$Asp98 O$^{\delta 2}$	6.04
*Ec*Pth	Gly111 O$\cdots$Asp96 O$^{\delta 2}$	5.97
*Ms*Pth	Gly113 C$^{\alpha}\cdots$Asp98 O$^{\delta 2}$	4.52
*Mt*Pth	Gly113 C$^{\alpha}\cdots$Asp98 O$^{\delta 2}$	3.33

out further manual model building. The additional cycles of refinement were also carried out to locate water oxygen atoms. The water oxygen atoms were placed at the electron density peaks in the $(F_o–F_c)$ map where the peaks were above 3σ and formed hydrogen bonds with protein atoms or with other water molecules. The B-factors were refined isotropically. Finally, the refinement converged to values of 0.168 and 0.198 for R_{cryst} and R_{free} factors, respectively. The structural validation was carried out using the program PROCHECK [42]. The final refined model consists of 2980 protein atoms and 281 water oxygen atoms. The data quality and final refinement statistics are reported in Table 1. The coordinates and structure factors have been deposited in the Protein Data Bank with accession code PDB: 4QT4.

Acknowledgements

Appendix A. Supplementary data

Supplementary data associated with this article can be found, in the online version, at http://dx.doi.org/10.1016/j.fob.2014.10.010.

References

[1] Manley, J.L. (1978) Synthesis and degradation of termination and premature-termination fragments of beta-galactosidase *in vitro* and *in vivo*. J. Mol. Biol. 125, 407–432.

[2] Jorgensen, F. and Kurland, C.G. (1990) Processivity errors of gene expression in *Escherichia coli*. J. Mol. Biol. 215, 511–521.

[3] Singh, N.S. and Varshney, U. (2004) A physiological connection between tmRNA and peptidyl-tRNA hydrolase functions in *Escherichia coli*. Nucleic Acids Res. 32, 6028–6037.

[4] Cruz-Vera, L.R1, Magos-Castro, M.A., Zamora-Romo, E. and Guarneros, G. (2004) Ribosome stalling and peptidyl-tRNA drop-off during translational delay at AGA codons. Nucleic Acids Res. 32, 4462–4468.

an oscillation range of 1° with an exposure time of 3 s per image using a wavelength of 0.98 Å. A total of 400 images were collected. The crystals diffracted to 2.19 Å resolution. The indexing of data indicated that the crystals belonged to space group P1 with unit cell dimensions, a = 36.0 Å, b = 43.0 Å, c = 65.1 Å, α = 90.3°, β = 105.7°, γ = 112.5°. The Matthews constant, V_m [35] of 2.0 Å^3/Da was calculated for two molecules in the asymmetric unit which corresponded to a solvent content of 41.3%. The data were processed with AUTOMAR and SCALEPACK from HKL package [36]. The summary of data collection and processing details is presented in Table 1.

4.4. Structure determination and refinement of SpPth

The structure of *Sp*Pth was determined with program Phaser [37] in CCP4i suite [38] using coordinates of *Ab*Pth (PDB: 4WH4) as the search model. The amino acid sequence identity between *Sp*Pth and *Ab*Pth was 32% (Fig. 1). The Phaser program gave a solution for two molecules in the asymmetric unit. The coordinates obtained from the output of calculations using Phaser program were subjected to several cycles of maximum likelihood refinement with REFMAC5 [39]. The whole chain was rebuilt, segment by segment, using omit maps which were calculated by removing segments of a protein chain followed by 10 cycles of refinement with REFMAC 5. The refined model was adjusted manually using programs, O [40] and COOT [41]. The structure gradually improved on fitting the protein molecule in electron density maps calculated with $(F_o–F_c)$ and $(2F_o–F_c)$ coefficients. This was followed by 10 rounds of refinement cycles. The model was improved by carrying

[5] Menninger, J.R. (1976) Peptidyl-transfer RNA dissociates during protein synthesis from ribosomes of *Escherichia coli*. J. Biol. Chem. 251, 3392–3398.

[6] Atherly, A.G. (1978) Peptidyl-transfer RNA hydrolase prevents inhibition of protein synthesis initiation. Nature 275, 769.

[7] Menninger, J.R. (1979) Accumulation of peptidyl tRNA is lethal to *Escherichia coli*. J. Bacteriol. 137, 694–696.

[8] Menez, J., Heurgué-Hamard, V. and Buckingham, R.H. (2000) Sequestration of specific tRNA species cognate to the last sense codon of an overproduced gratuitous protein. Nucleic Acids Res. 28, 4725–4732.

[9] Atherly, A.G. and Menninger, J.R. (1972) Mutant *E. coli* strain with temperature sensitive peptidyl-transfer RNA hydrolase. Nat. New Biol. 240, 245–246.

[10] Cuzin, F., Kretchmer, N., Greenberg, R.E., Hurwitz, R. and Chapeville, F. (1967) Enzymatic hydrolysis of N-substituted aminoacyl-tRNA. Proc. Natl. Acad. Sci. U.S.A. 58, 2079–2086.

[11] Kössel, H. and RajBhandary, U.L. (1968) Studies on polynucleotides. LXXXVI. Enzymic hydrolysis of N-acylaminoacyl-transfer RNA. J. Mol. Biol. 35, 539–560.

[12] Jost, J.P. and Bock, R.M. (1969) Enzymatic hydrolysis of N-substituted aminoacyl transfer ribonucleic acid in yeast. J. Biol. Chem. 244, 5866–5873.

[13] McShan, W.M., Ferretti, J.J., Karasawa, T., Suvorov, A.N., Lin, S., Qin, B., Jia, H., Kenton, S., Najar, F., Wu, H., et al. (2008) Genome sequence of a nephritogenic and highly transformable M49 strain of *Streptococcus pyogenes*. J. Bacteriol. 190, 7773–7785.

[14] Dujeancourt, L., Richte, R., Chrzanowska-Lightowlers, Z.M., Bonnefoy, N. and Herberta, C.J. (2013) Interactions between peptidyl tRNA hydrolase homologs and the ribosomal release factor Mrf1 in *S. pombe* mitochondria. Mitochondrion 13, 871–880.

[15] Kossel, H. (1970) Purification and properties of peptidyl-tRNA hydrolase from *Escherichia coli*. Biochim. Biophys. Acta 204, 191–202.

[16] Brun, G., Paulin, D., Yot, P. and Chapeville, F. (1971) Peptidyl-tRNA hydrolase: demonstration in various organisms. Enzymatic activity in the presence of ribosomes. Biochimie 53, 225–231.

[17] Menez, J., Buckingham, R.H., De Zamaroczy, M. and Campelli, C.K. (2002) Peptidyl-tRNA hydrolase in *Bacillus subtilis*, encoded by spoVC, is essential to vegetative growth, whereas the homologue enzyme in *Saccharomyces cerevisiae* is dispensable. Mol. Microbiol. 45, 123–129.

[18] Rosas-Sandoval, G., Ambrogelly, A., Rinehart, J., Wei, D., Cruz-Vera, L.R., Graham, D.E., Stetter, K.O., Guarneros, G. and Söll, D. (2002) Orthologs of a novel archaeal and of the bacterial peptidyl-tRNA hydrolase are nonessential in yeast. Proc. Natl. Acad. Sci. U.S.A. 99, 16707–16712.

[19] Fromant, M., Ferri-Fioni, M.L., Plateau, P. and Blanquet, S. (2003) Peptidyl-tRNA hydrolase from *Sulfolobus solfataricus*. Nucleic Acids Res. 31, 3227–3235.

[20] Powers, R., Mirkovic, N., Goldsmith-Fischman, S., Acton, T.B., Chiang, Y., Huang, Y.J., Ma, L., Rajan, P.K., Cort, J.R., Kennedy, M.A., et al. (2005) Solution structure of *Archaeoglobus fulgidus* peptidyl-tRNA hydrolase (Pth2) provides evidence for an extensive conserved family of Pth2 enzymes in archaea, bacteria, and eukaryotes. Protein Sci. 14, 2849–2861.

[21] Fromant, M., Schmitt, E., Mechulam, Y., Lazennec, C., Plateau, P. and Blanquet, S. (2005) Crystal structure at 1.8 Å resolution and identification of active site residues of *Sulfolobus solfataricus* peptidyl-tRNA hydrolase. Biochemistry 44, 4294–4301.

[22] Shimizu, K., Kuroishi, C., Sugaharac, M. and Kunishima, N. (2008) Structure of peptidyl-tRNA hydrolase 2 from *Pyrococcus horikoshii* OT3: insight into the functional role of its dimeric state. Acta Crystallogr. D 64, 444–453.

[23] De-Pereda, J.M., Waas, W.F., Jan, Y., Ruoslahti, E., Schimmel, P. and Pascual, J. (2004) Crystal structure of a human peptidyl-tRNA hydrolase reveals a new fold and suggests basis for a bifunctional activity. J. Biol. Chem. 279, 8111–8115.

[24] Schmitt, E., Mechulam, Y., Fromant, M., Plateau, P. and Blanquet, S. (1997) Crystal structure at 1.2 Å resolution and active site mapping of *Escherichia coli* peptidyl-tRNA hydrolase. EMBO J. 16, 4760–4769.

[25] Kaushik, S., Singh, N., Yamini, S., Singh, A., Sinha, M., Arora, A., Kaur, P., Sharma, S. and Singh, T.P. (2013) The mode of inhibitor binding to peptidyl-tRNA hydrolase: binding studies and structure determination of unbound and bound peptidyl-tRNA hydrolase from *Acinetobacter baumannii*. PLoS ONE 8, e67547.

[26] Hughes, R.C., McFeeters, H., Coates, L. and McFeeters, R.L. (2012) Recombinant production, crystallization and X-ray crystallographic structure determination of the peptidyl-tRNA hydrolase of *Pseudomonas aeruginosa*. Acta Crystallogr. Sect. F 68, 1472–1476.

[27] Singh, A., Kumar, A., Gautam, L., Sharma, P., Sinha, M., Bhushan, A., Kaur, P., Sharma, S., Arora, A. and Singh, T.P. (2014) Structural and binding studies of peptidyl-tRNA hydrolase from *Pseudomonas aeruginosa* provide a platform for the structure based inhibitor design against peptidyl-tRNA hydrolase. Biochem. J. 463, 329–337.

[28] Clarke, T.E., Romanov, V., Lam, R., Gothe, S.A., Peddi, S.R., Razumova, E.B., Lipman, R.S., Branstrom, A.A. and Chirgadze, N.Y. (2011) Structure of *Francisella tularensis* peptidyl-tRNA hydrolase. Acta Crystallogr. Sect. F 67, 446–449.

[29] Baugh, L., Gallagher, L.A., Patrapuvich, R., Clifton, M.C., Gardberg, A.S., Edwards, T.E., Armour, B., Begley, D.W., Dieterich, S.H., Dranow, D.M., et al. (2013) Combining functional and structural genomics to sample the essential *Burkholderia structome*. PLoS ONE 8, e53851.

[30] Selvaraj, M., Roy, S., Singh, N.S., Sangeetha, R., Varshney, U. and Vijayan, M. (2007) Structural plasticity and enzyme action: crystal structures of *Mycobacterium tuberculosis* peptidyl-tRNA hydrolase. J. Mol. Biol. 372, 186–193.

[31] Kumar, A., Singh, N., Yadav, R., Kumar, R.P., Sharma, S., Arora, A. and Singh, T.P. (2012) Crystal structure of peptidyl-tRNA hydrolase from *Mycobacterium smegmatis* reveals novel features related to enzyme dynamics. Int. J. Biochem. Mol. Biol. 23, 58–69.

[32] Fromant, M., Plateau, P., Schmitt, E., Mechulam, Y. and Blanquet, S. (1999) Receptor site for the 5′-phosphate of elongator tRNAs governs substrate selection by peptidyl-tRNA hydrolase. Biochemistry 38, 4982–4987.

[33] Goodall, J.J., Chen, G.J. and Page, M.G.P. (2004) Essential role of histidine 20 in the catalytic mechanism of *Escherichia coli* peptidyl-tRNA hydrolase. Biochemistry 43, 4583–4591.

[34] Ito, K., Murakami, R., Mochizuki, M., Qi, H., Shimizu, Y., Miura, K., Ueda, T. and Uchiumi, T. (2012) Structural basis for the substrate recognition and catalysis of peptidyl-tRNA hydrolase. Nucleic Acids Res. 40, 10521–10531.

[35] Matthews, B.W. (1968) Solvent content of protein crystals. J. Mol. Biol. 33, 491–497.

[36] Otwinowski, Z. and Minor, W. (1997) Processing of X-ray diffraction data collected in oscillation mode. Methods Enzymol. 276, 307–326.

[37] McCoy, A.J., Grosse-Kunstleve, R.W., Adams, P.D., Winn, M.D., Storoni, L.C. and Read, R.J. (2007) Phaser crystallographic software. J. Appl. Crystallogr. 40, 658–674.

[38] Winn, M.D., Ballard, C.C., Cowtan, K.D., Dodson, E.J., Emsley, P., Evans, P.R., Keegan, R.M., Krissinel, E.B., Leslie, A.G., McCoy, A., et al. (2011) Overview of the CCP4 suite and current developments. Acta Crystallogr. D 67, 235–242.

[39] Murshudov, G.N., Skubak, P., Lebedev, A.A., Pannu, N.S., Steiner, R.A., Nicholls, R.A., Winn, M.D., Long, F. and Vagin, A.A. (2011) REFMAC5 for the refinement of macromolecular crystal structures. Acta Crystallogr. D 67, 355–367.

[40] Jones, T.A., Zou, J.Y., Cowan, S.W. and Kjeldgaard, M. (1991) Improved methods for building protein models in electron density maps and the location of errors in these models. Acta Crystallogr. A 47, 110–119.

[41] Emsley, P. and Cowtan, K. (2004) Coot: model-building tools for molecular graphics. Acta Crystallogr. D 60, 2126–2132.

[42] Laskowski, R.A., MacArthur, M.W., Moss, D.S. and Thornton, J.M. (1993) PROCHECK: a program to check stereo chemical quality of protein structures. J. Appl. Crystallogr. 26, 283–291.